2008-12

Exploiting distinct molecular architectures of ultrathin films made with iron phthalocyanine for sensing

Journal of Physical Chemistry B,Washington, DC, v. 112, n. 48, p. 15275-15282, Dec. 2008
http://www.producao.usp.br/handle/BDPI/49242

THE JOURNAL OF PHYSICAL CHEMISTRY B

Article

Exploiting Distinct Molecular Architectures of Ultrathin Films Made with Iron Phthalocyanine for Sensing

D. Volpati, P. Alessio, A. A. Zanfolim, F. C. Storti, A. E. Job, M. Ferreira, A. Riul Jr, O. N. Oliveira Jr, and C. J. L. Constantino

J. Phys. Chem. B, **2008**, 112 (48), 15275-15282 • DOI: 10.1021/jp804159h • Publication Date (Web): 06 November 2008

Exploiting Distinct Molecular Architectures of Ultrathin Films Made with Iron Phthalocyanine for Sensing

D. Volpati,[†] P. Alessio,[†] A. A. Zanfolim,[†] F. C. Storti,[†] A. E. Job,[†] M. Ferreira,[‡] A. Riul, Jr,[‡] O. N. Oliveira, Jr,[§] and C. J. L. Constantino*[,†]

DFQB, FCT, UNESP, CP 467, 19060-900, Presidente Prudente, SP, Brazil, Universidade Federal de São Carlos, 18043-970, campus Sorocaba, SP, Brazil, and Instituto de Física de São Carlos, USP, 13560-970, São Carlos, SP, Brazil

Received: May 11, 2008; Revised Manuscript Received: August 31, 2008

The possibility of generating distinct film properties from the same material is crucial for a number of applications, which can only be achieved by controlling the molecular architecture. In this paper we demonstrate as a proof-of-principle that ultrathin films produced from iron phthalocyanine (FePc) may be used to detect trace amounts of copper ions in water, where advantage was taken of the cross sensitivity of the sensing units that displayed distinct electrical properties. The ultrathin films were fabricated with three methods, namely physical vapor deposition (PVD), Langmuir−Blodgett (LB), and electrostatic layer-by-layer (LbL) techniques, where for the latter tetrasulfonated phthalocyanine was used (FeTsPc). PVD and LB films were more homogeneous than the LbL films at both microscopic and nanoscopic scales, according to results from micro-Raman spectroscopy and atomic force microscopy (AFM), respectively. From FTIR spectroscopy data, these more homogeneous films were found to have FePc molecules oriented preferentially, tilted in relation to the substrate surface, while FeTsPc molecules were isotropically distributed in the LbL films. Impedance spectroscopy measurements with films adsorbed onto interdigitated gold electrodes indicated that the electrical response depends on the type of film-forming method and varies with incorporation of copper ions in aqueous solutions. Using principal component analysis (PCA), we were able to exploit the cross sensitivity of the sensing units and detect copper ions (Cu^{2+}) down to 0.2 mg/L, not only in ultrapure water but also in distilled and tap water. This level of sensitivity is sufficient for quality control of water for human consumption, with a fast, low-cost method.

Introduction

Phthalocyanines are semiconducting, organic molecules with a general formula $C_{32}H_{16}N_8$, which possess a centrosymmetric, planar structure with various polymorphic forms.[1] They are hardly soluble in organic solvents, but solubility and processability may be enhanced by incorporation of functional groups to the macrocycle. The electrical and optical properties of phthalocyanines are highly sensitive to the environment, especially in the case when they form bisphthalocyanines with a metal complexed in the macrocycle.[2,3] Among their many useful properties are included chemical and thermal stability, photoconductivity, electrochromism, photochemical and photosynthetic activities, luminescence,[2−4] nonlinear optical characteristics, and ability of optical storage.[3,5] In industry, phthalocyanines are widely used as dyes for textiles and for coating metallic surfaces. There is now a surge on their use for devices, for example, in photocopiers, solar cells, electrochromic displays, fuel cells, light-emitting diodes, transistors, optical limiters, in photodynamic therapy,[6−18] and sensors.[15,19−21]

In several of the possible applications, one important requirement is to produce materials in the form of thin films, which has been carried out for phthalocyanines with various methods, including Langmuir−Blodgett (LB),[22−26] electrostatic layer-by-layer (LbL),[27−30] physical vapor deposition (PVD),[31,32] and casting.[33] For sensing, in particular, it has been shown that film morphology and surface properties are relevant for the sensor performance.[20] While such dependence makes it difficult to analyze experimental results for the sensors, it opens the way to obtain distinct electrical and optical properties from the same phthalocyanine molecule, but using different film-forming methods or experimental conditions.

In this study, we selected iron phthalocyanine (FePc) to produce LB and PVD films, while LbL films were fabricated with tetrasulfonated iron phthalocyanine (FeTsPc). The tetrasulfonation in this case was essential to make the material water soluble, as required for the LbL method. The film growth was characterized using UV−vis absorption spectroscopy, and film morphology was assessed at the microscopic level, with optical microscope and micro-Raman spectroscopy, and at the nanoscopic level with atomic force microscopy (AFM). The organization of the molecules in the films was probed with FTIR absorption spectroscopy in the transmission and reflection modes. As we shall show, the film properties varied with the method of fabrication, and this allowed the cross sensitivity of sensing units to be used in detecting trace amounts of copper ions (Cu^{2+}) in aqueous solutions, using impedance spectroscopy.

Experimental Methods

Fabrication of Ultrathin Films. The LbL films of FeTsPc were grown from 5.0 mg/mL of PAH (Aldrich) and 5.0 mg/mL of FeTsPc (Aldrich) aqueous solutions, prepared with

* To whom correspondence should be addressed. E-mail: case@fct.unesp.br.
† DFQB, FCT, UNESP.
‡ Universidade Federal de São Carlos, campus Sorocaba.
§ Instituto de Física de São Carlos, USP.

10.1021/jp804159h CCC: $40.75
Published on Web 11/06/2008

ultrapure water (18.2 MΩ.cm) from a Milli-Q system model Simplicity. The multilayer LbL films were made by immersing the substrate alternately into the cationic poly(allylamine hydrochloride) (PAH) and anionic (FeTsPc) solutions for 3 min. After each deposition step, the films were rinsed with the washing solution and dried in moderated air flow. The number of bilayers and the substrate for each film used in distinct characterization methods differed. Films with 15 bilayers were adsorbed onto quartz for UV−vis absorption spectroscopy. For FTIR spectroscopy, 30 bilayers were deposited onto ZnSe and 63 bilayers were adsorbed onto an Ag mirror for transmission and reflection modes, respectively. For the measurements of impedance spectroscopy, Au interdigitated electrodes were coated with five bilayers of PAH/FeTsPc, while in AFM measurements glass was covered with five bilayers. The reason why different numbers of layers were used for characterizing the LbL and LB films with distinct techniques was to match with the sensitivity of these techniques.

The PVD films of FePc (Kodak) were grown using a Boc Edwards vacuum system model Auto 306. The FePc powder was placed into a metallic boat of Ta (melting point at 3014 °C), which is heated by an electrical current at 10^{-6} Torr. The thickness of the FePc evaporated film was controlled with a quartz crystal balance. The electrical current was adjusted slowly to 2.2 A (10 V) until the boat reached 400 °C. This careful electrical current adjustment is required for controlling the deposition ratio and preventing the material from "blowing up", which leads to a loss of thickness and morphology control. PVD films were grown with 10, 20, 30, 40, and 50 nm mass thicknesses onto glass substrates for UV−vis absorption spectroscopy, 36 nm onto ZnSe and Ag mirror for FTIR spectroscopy (transmission and reflection modes, respectively), 10 nm onto Au interdigitated electrodes for impedance spectroscopy and onto glass for AFM. The identical Raman spectra of both powder and PVD films confirm that the chemical structure of the FePc molecule is not affected during the evaporation process (figure not shown).

The LB films of FePc were grown using a KSV Langmuir trough model 2000. A solution with 3.1 mg of FePc (MW = 568.38 g/mol, Kodak) in 10 mL of chloroform (MW = 119.38 g/mol, Merck) was spread onto ultrapure water with a microsyringe. The monolayer thus formed at the air/water interface was compressed with a barrier speed of 10 mm/min, and transfer onto solid substrates was performed at a surface pressure of 25 mN/m, corresponding to the liquid-condensed state, thus forming the so-called LB films (Y-type). Before immersing the substrate into the water subphase, 15 min elapsed for drying the LB layer deposited previously. When inside the water subphase, the waiting time was 30 s. The substrate speed varied between 0.5 and 3.5 mm/min being manually adjusted during the deposition to keep the cumulative transfer curve close to one. With this procedure, one ensures not only that a similar amount of material was transferred per layer but also that the material was transferred homogeneously onto the substrate. The cumulative transfer curve is given by the ratio between the area scanned by the barriers to keep the surface pressure constant during LB deposition and the covered area of the substrate. LB films were deposited which contained 3, 5, 10, and 15 layers onto quartz substrates for UV−vis absorption, 25 layers onto ZnSe and Ag mirror for FTIR measurements (transmission and reflection modes, respectively), 5 layers onto Au interdigitated electrodes for impedance spectroscopy and onto glass for AFM.

Film Characterization Methods. The UV−vis absorption spectroscopy was carried out using a spectrophotometer Varian model Cary 50. The FTIR measurements were taken with a spectrometer Bruker model Vector 22 equipped with DTGS detector. FTIR spectra were recorded for FePc in KBr pellet and FeTsPc cast film, used as references, with resolution of 4 cm^{-1} and 64, 256, and 512 scans. For the ultrathin films, namely PVD, LB, and LbL films, N_2 was purged to decrease CO_2 and water vapor interference. An accessory Bruker model A518/Q was used with the incident IR light angle at 80° in the reflection mode. The Raman spectra were obtained with a spectrograph Renishaw model in-Via, which is coupled to a Leica optical microscope allowing recording spectra point-by-point with spatial resolution of ca. 1 μm^2 using an objective of 50× magnification, and CCD detector. The 633 nm laser line was used, which is in resonance with FePc and FeTsPc UV−vis absorption spectra, in order to achieve the so-called resonance Raman scattering (RRS). The grating employed had 1800 L/mm yielding a spectral resolution of ca. 4 cm^{-1}. With an *XYZ*-motorized stage, Raman images could be obtained by collecting the spectra along an area or line previously chosen for the mapping. The AFM images were collected using a Digital Instrument model Nanoscope IV with a tip of silicon nitride, spring constant of 0.12 N/m, and distance tip−sample surface varying between 20 and 50 nm.

Impedance Spectroscopy. The impedance spectroscopy measurements were carried out using a Solartron impedance system model 1260A. The Au electrodes used in the sensing units possess 50 fingers with 10 μm of width, 5 mm of length, and 100 nm of height, with 10 μm of distance between each finger. The capacitance values were recorded using an input signal at 50 mV of amplitude with frequency interval between 1 Hz and 1 MHz. The measurements were performed in ultrapure, distilled, and tap water and solutions of Cu^{2+} (from $CuCl_2$) at 0.2, 2.0, and 20.0 mg/L concentration (pH of ultrapure water = 5.6 (5.1 for 20.0 mg/L Cu^{2+}); distilled water = 6.8 (6.1 for 20.0 mg/L Cu^{2+}); tap water = 8.9 (7.4 for 20.0 mg/L Cu^{2+})). These concentrations were chosen since 5.0 mg/L is the standard threshold established by the Brazilian regulation for an unacceptable concentration of Cu^{2+} in potable water.

The Au electrodes were covered with PAH/FeTsPc (LbL) and FePc (PVD and LB) ultrathin films and immersed into each liquid for 20 min to reach a stable electrical response. The measurements were started in water (ultrapure or distilled or tap) without Cu^{2+} ions. In the sequence, the measurements were carried out in solutions with Cu^{2+} ions, from lower to higher concentrated solutions. Between each measurement, the sensing units were washed with ultrapure water and dried before immersing into the initial water (ultrapure or distilled or tap) to check if the capacitance value was close to those previously measured at the same water background. Each measurement was recorded at 23 °C with five sequential scanning procedures over the whole frequency range.

Results and Discussion

Our goal in performing a detailed characterization of ultrathin films from iron phthalocyanine produced with different techniques is 2-fold. First, we wish to establish how experimental conditions and film architecture may affect the final film properties. Second, because our expectation - which was actually fulfilled as shown in this section - is that diverse film properties may emerge, we shall employ the ultrathin films as sensing units with cross sensitivity to detect trace amounts of copper ions in aqueous solutions.

Film Growth Assessed with UV−Visible Absorption Spectroscopy. The growth of LbL, PVD, and LB films was monitored with UV−vis absorption spectroscopy, whose spectra

are shown in Figure 1 panels A, B, and C, respectively. The molecular structures of FeTsPc and PAH are displayed in Figure 1A while that of FePc appears in Figure 1B. LbL films of PAH/FeTsPc with up to 15 bilayers, PVD films of FePc with 10, 20, 30, 40, and 50 nm mass thickness, and LB films with 3, 5, 10, and 15 layers were fabricated. In all cases a linear growth of the absorbance with the deposited LbL bilayers, PVD mass thickness, and LB layers was observed as shown in Figure 2 panels A, B, and C, respectively. This shows that the same amount of material was transferred onto the substrates, within the dispersion of the data obtained here.

The absorption in the UV−vis spectra of the PAH/FeTsPc LbL films in Figure 1A is assigned to FeTsPc since PAH does not absorb at this wavelength range. The characteristic bands B at lower wavelengths and Q at higher wavelengths, which are attributed to the electronic transitions HOMO→LUMO ($\pi \rightarrow \pi^*$),[1] are also seen. FeTsPc is more aggregated in the LbL film than in solution, as indicated by the red shift in the spectra compared to the spectrum in solution. The Q-band in Figure 1B,C, between 500 and 900 nm in the spectra of FePc, displays an overlapping of 3 main bands (shoulders) with maxima at 570, 630, and 710 nm for the PVD film and 590, 675, and 755 nm for the LB film. Usually, when there are only two bands in the wavelength range considered above, the band at lower wavelength is assigned to dimers while the other is attributed to monomers.[13] In our case, the third maximum and the difference in energy between these maxima (within tenths of eV) suggest transitions from the fundamental to different vibrational levels of the first electronic excited state. Furthermore, the red shift in the maximum absorption for LB films in relation to PVD films suggests distinct molecular organizations and/or molecular aggregate formation (J and H types), although the molecule is the same.[25,26,32,34]

Film Morphology at Micrometer and Nanometer Scales. The morphology at micrometer and nanometer scales of LbL, PVD, and LB films was investigated through micro-Raman spectroscopy and AFM. Figure 3 panels A, B, and C show at the top optical images and Raman mappings for the PAH/FeTsPc LbL film with 20 bilayers, FePc PVD with 30 nm mass thickness, and FePc LB with 21 layers, respectively. Marks were made in the optical images in Figure 3A,B to indicate two lines of 100 μm where Raman spectra were collected point-by-point with a step of 1 μm. These lines are the 2-dimensional Raman mappings where the brighter spots indicate stronger Raman signals for the band at 750 cm^{-1} assigned to C−H wagging.[25,26] All the 101 Raman spectra collected along that line are given at the top right corner forming the 3-dimensional Raman mappings. Figure 3C presents a similar result, but with the Raman spectra collected along an area (instead of a line) of 50 μm x 50 μm with a step of 5 μm leading to a total of 121 spectra (one of these spectra is shown at the top right corner in Figure 3C). Again, the brighter spots indicate a stronger Raman signal for the band at 1515 cm^{-1} assigned to C═N pyrrole stretching,[25,26] which is shown in the spectrum at the top right corner. Overall, the FePc PVD and LB films seem to be the more homogeneous at the micrometer scale while the LbL would be the less homogeneous one accordingly to the optical images. However, from the Raman mappings and considering that the Raman signal intensities are proportional to the quantity of material, it can be concluded that the PVD film is the most homogeneous followed by LB and LbL films.

Figures 3 panels A, B, and C display at the bottom topographic AFM images for the five-bilayer PAH/FeTsPc LbL film, FePc PVD film with 10 nm mass thickness, and five-layer

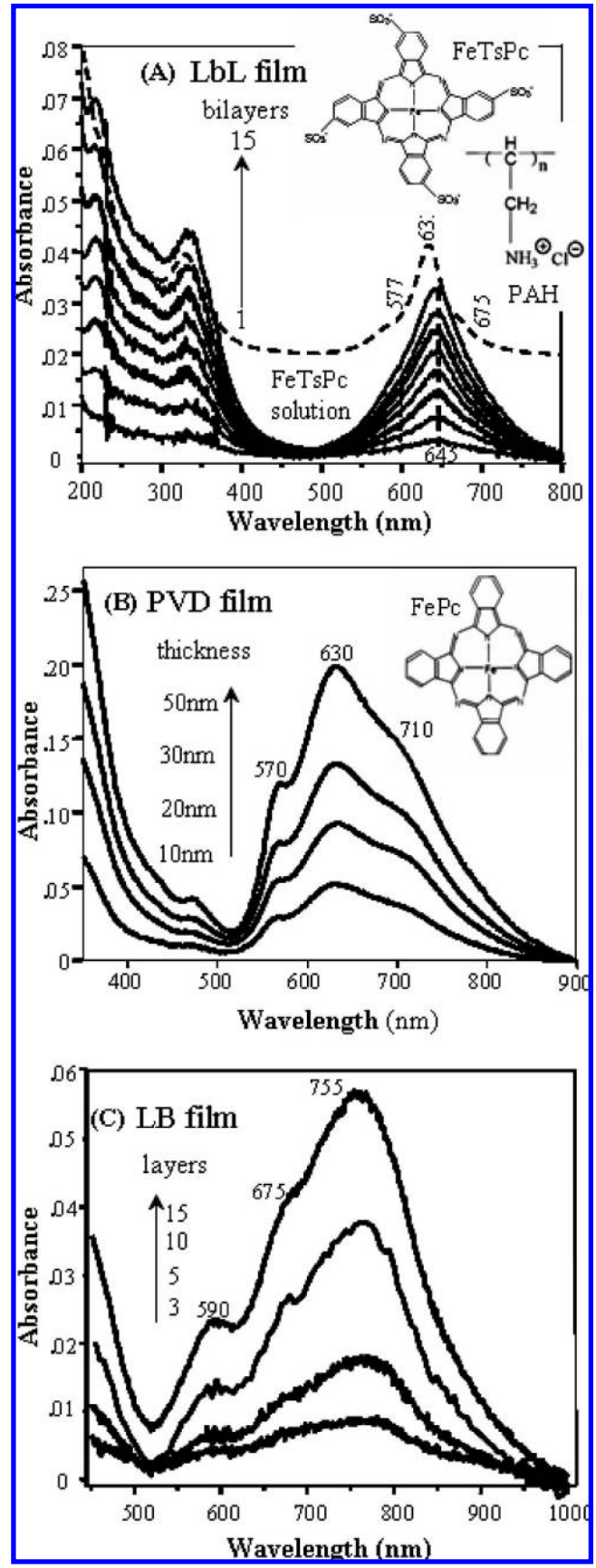

Figure 1. UV−vis absorption spectra for (A) PAH/FeTsPc LbL films for different number of bilayers and the UV−vis absorption spectrum for FeTsPc aqueous solution (the scale in the *Y*-axis refers to LbL films); (B) FePc PVD films for different mass thicknesses; (C) FePc LB films for different number of layers. The molecular structures of FeTsPc and PAH are given in the inset in panel A and FePc in panel B.

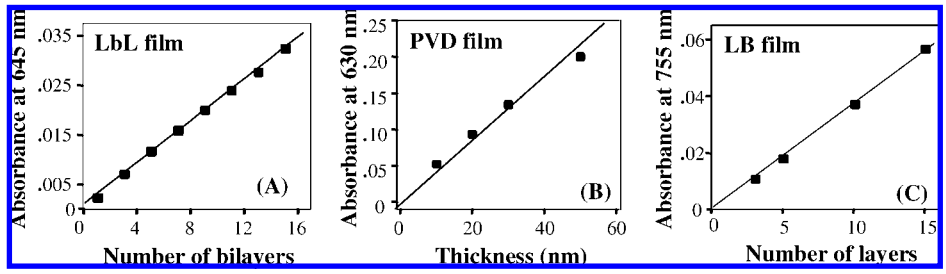

Figure 2. (A) Absorbance at 645 nm vs number of LbL bilayers; (B) absorbance at 630 nm vs PVD mass thickness; (C) absorbance at 755 nm vs number of LB layers.

FePc LB film, respectively. These samples were chosen to be coincident in number of bilayers (LbL), thickness (PVD), and layers (LB) with those investigated using impedance spectroscopy in the sensing units. The AFM images at the right bottom corner illustrate the film surface morphology with a profile produced by scratching the films, which allowed determination of the average thickness. The measurements revealed good agreement between the thickness measured by AFM and by quartz crystal balance in the PVD film growth. For the LbL films an average thickness of 1 nm per bilayer was found, consistent with the thickness measured by profilometry for a PAH/FeTsPc LbL film with 55 bilayers.[13] For the LB film the average thickness was 1.8 nm per layer. The AFM images feature molecular aggregates onto film surfaces, which are analyzed in diameter and number of aggregates. While PVD films exhibit the largest aggregates, followed by LB, and LbL films, this trend is inverted with regard to the number of aggregates.

Molecular Organization Investigated with FTIR Spectroscopy. The investigation of molecular organization in the ultrathin films was carried out through FTIR in transmission and reflection modes. Figure 4A displays the FTIR spectra for the cast film of (PAH + FeTsPc) to be taken as reference (transmission mode), and for the LbL films of PAH/FeTsPc with 30 bilayers onto ZnSe and 63 bilayers onto an Ag mirror, for transmission and reflection modes, respectively. The similarity between the FTIR spectra reveals that the LbL films are isotropic with regard to molecular organization. The spectrum of an LbL film is not merely a superposition of the spectra of the film components (PAH and FeTsPc—figure not shown, see ref 29 and references therein). Of particular relevance are the bands at 1025, 1181, and 1213 cm^{-1} related to SO_3 stretching, whose relative intensity points to an intimate contact between NH_3^+ groups in PAH and SO_3^- groups in FeTsPc.[29]

Figure 4B shows the FTIR spectra for a PVD film of FePc with 36 nm of mass thickness and FePc in KBr pellet as reference. The bands at 729 cm^{-1} are attributed to C−H wagging (FePc macrocycle out-of-plane), while the bands at 1117 and 1331 cm^{-1} are assigned, respectively, to C−H in-plane deformation and C═C or C═N stretching (pyrrol), also in the plane of the FePc macrocycle.[25,26,31,32] The C−H wagging is relatively intense in all the spectra (KBr pellet and PVD films), and dominates the FTIR-reflection spectrum. This difference in the relative intensity for the transmission and reflection modes reveals anisotropy in the molecular organization of FePc in the PVD films. Differences in the relative intensity also appear when comparing the transmission and reflection FTIR spectra for the LB film of FePc in Figure 4C, which point to anisotropic films with predominance of the band at 729 cm^{-1} in the reflection spectrum while the transmission mode is dominated by the band at 1331 cm^{-1}.

The molecular organization can be determined from the FTIR spectra and the surface selection rules which take into account basically two pieces of information:[35−40] (i) the intensity (I) of the infrared absorption for a fixed molecule in the space depends on the scalar product between the electric field of the incident radiation ($\vec{E}$) and the transient dipole moment of each vibrational mode of the molecule ($\vec{\mu}'$) such that $I = \vec{E}\,\vec{\mu}'$; (ii) in transmission mode the incident electric field is parallel to the substrate surface while in reflection mode it is polarized perpendicularly to the substrate surface for the metal (Ag) and incident angle (80°) used here. Therefore, the combination of measurements in transmission and reflection modes allows the molecular organization to be determined using FTIR bands whose $\vec{\mu}'$ components are well established.

Considering the decrease in relative intensity of the band at 729 cm^{-1} in the FTIR-reflection spectrum of FePc PVD film, and that this vibrational mode is perpendicular to the FePc macrocycle plane, one can infer using the surface selection rules that FePc molecules are tilted between 45 and 90° in relation to the substrate (inset in Figure 4B). Using the same procedure for the relative intensity of 729 cm^{-1} band for the FePc LB film, the FePc molecules are found to be tilted between 0 and 45 ° in relation to the substrate (inset in Figure 4C). The higher relative intensity in the FTIR-transmission spectrum for the LB film of the 1117 and 1331 cm^{-1} bands, whose vibrational modes are in the plane of the FePc macrocycle, corroborates the molecular orientation of FePc. This difference in the molecular orientation for FePc in PVD and LB films might be the reason for the shift in the absorption bands in the UV−vis spectra of Figures 1B and 1C.

It is interesting that the most homogeneous films, namely PVD and LB films, are also organized with the molecules in a preferential orientation, while the least homogeneous LbL films have the molecules randomly oriented. This can be ascribed to the type of film-forming technique or to the molecules used to fabricate the films, as the LB and PVD films were produced with FePc and the LbL films were obtained with FeTsPc. An inspection through the literature for phthalocyanines films indicates that both factors may be important. For PVD films, Aroca and co-workers[31,32,41,42] and other authors[43−45] have shown that the molecules are normally oriented preferentially, but this orientation depends on the metal incorporated in the phthalocyanine molecule as well as on experimental conditions for film fabrication, such as rate of deposition and substrate temperature. For LB and LbL films, there are fewer studies on molecular orientation. Again, molecular orientation induced in LB films depends on the metal and fabrication conditions, such as surface pressure of deposition and dipper speed.[46−53] In contrast to the lack of orientation in the LbL films studied here, Zucolotto et al.[29]reported preferential orientation for FeTsPc (the same molecule of the present study), but with the films being fabricated at a different pH. Because the pH of the solutions employed in the adsorption process of the LbL films governs the electrostatic interactions, film morphology may differ substantially with a change in pH.[29,30,54−57]

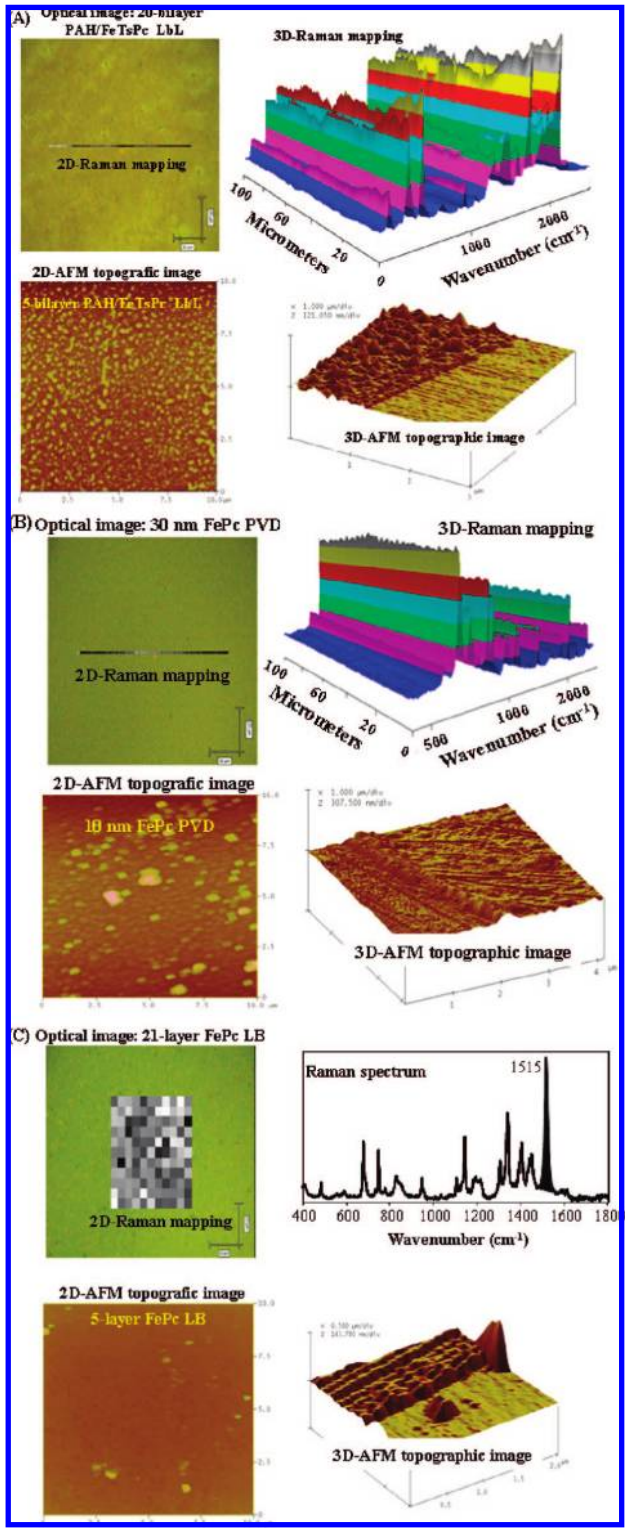

Figure 3. (A) Optical image (50×) superposed to the 2D-Raman mapping (top left corner) and 3D-Raman mapping (top right corner) for PAH/FeTsPc LbL film with 20 bilayers. Topographic AFM images for the PAH/FeTsPc LbL film with five bilayers in 2-dimension (bottom left corner) and 3-dimension (bottom right corner revealing a profile produced by scratching the film). (B) Optical image (50×) superposed to the 2D-Raman mapping (top left corner) and 3D-Raman mapping (top right corner) for FePc PVD film with 30 nm. Topographic AFM images for the FePc PVD film with 10 nm in 2-dimension (bottom left corner) and 3-dimension (bottom right corner revealing a profile produced by scratching the film). (C) Optical image (50×) superposed to the 2D-Raman mapping (top left corner) and a Raman spectrum collected with the 633 nm laser line (top right corner) for FePc LB film with 21 layers. Topographic AFM images for the FePc LB film with five layers in 2-dimension (bottom left corner) and 3-dimension (bottom right corner revealing a profile produced by scratching the film).

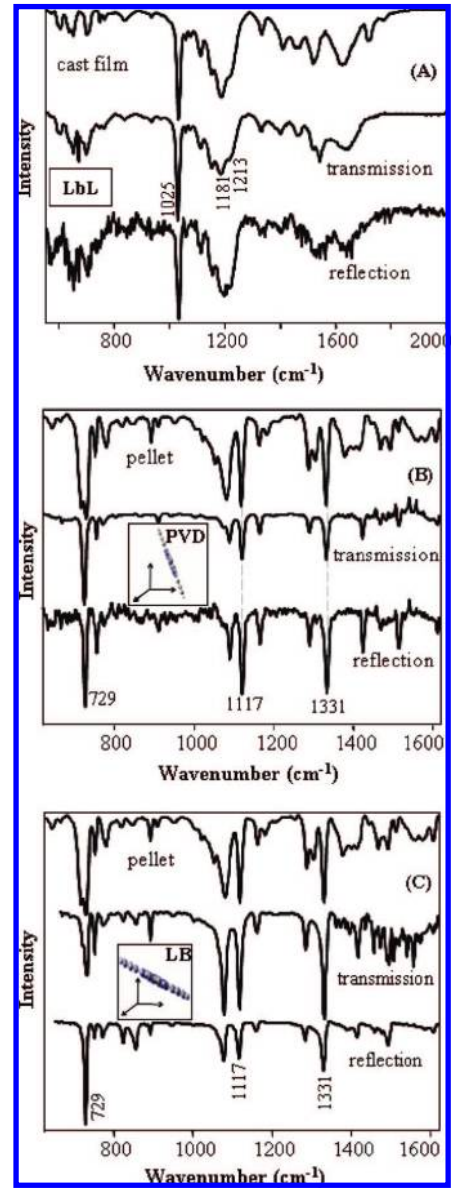

Figure 4. FTIR spectra (A) in the transmission mode for the (FeTsPc + PAH) cast film and 30-bilayer PAH/FeTsPc LbL film and in the reflection mode for the 63-bilayer PAH/FeTsPc LbL film; (B) in the transmission mode for the FePc in KBr pellet and 36 nm FePc PVD film and in the reflection mode for the 36 nm FePc PVD film; (C) in the transmission mode for the FePc in KBr pellet and 25-layer FePc LB film and in the reflection mode for the 25-layer FePc LB film.

From the analysis above, we conclude that molecular orientation may be induced with any of the three film-fabrication methods used here, which will depend on the choice of molecules, metal incorporated, and experimental conditions. While this poses difficulties for characterizing and interpreting the data of ultrathin films, it also represents an opportunity to exploit molecular control in the films, which may lead to diversified properties for films obtained with the same materials. Indeed, this is precisely what we have done in the present work, using the films as sensing units, as discussed below.

Applying the Ultrathin Films as Sensing Units. One of the most common applications of phthalocyanine films has been in sensors for gases and liquids, especially because the optical and electrical properties of these films are strongly dependent on the environment.[1−3,15,58] Several methods may be employed in

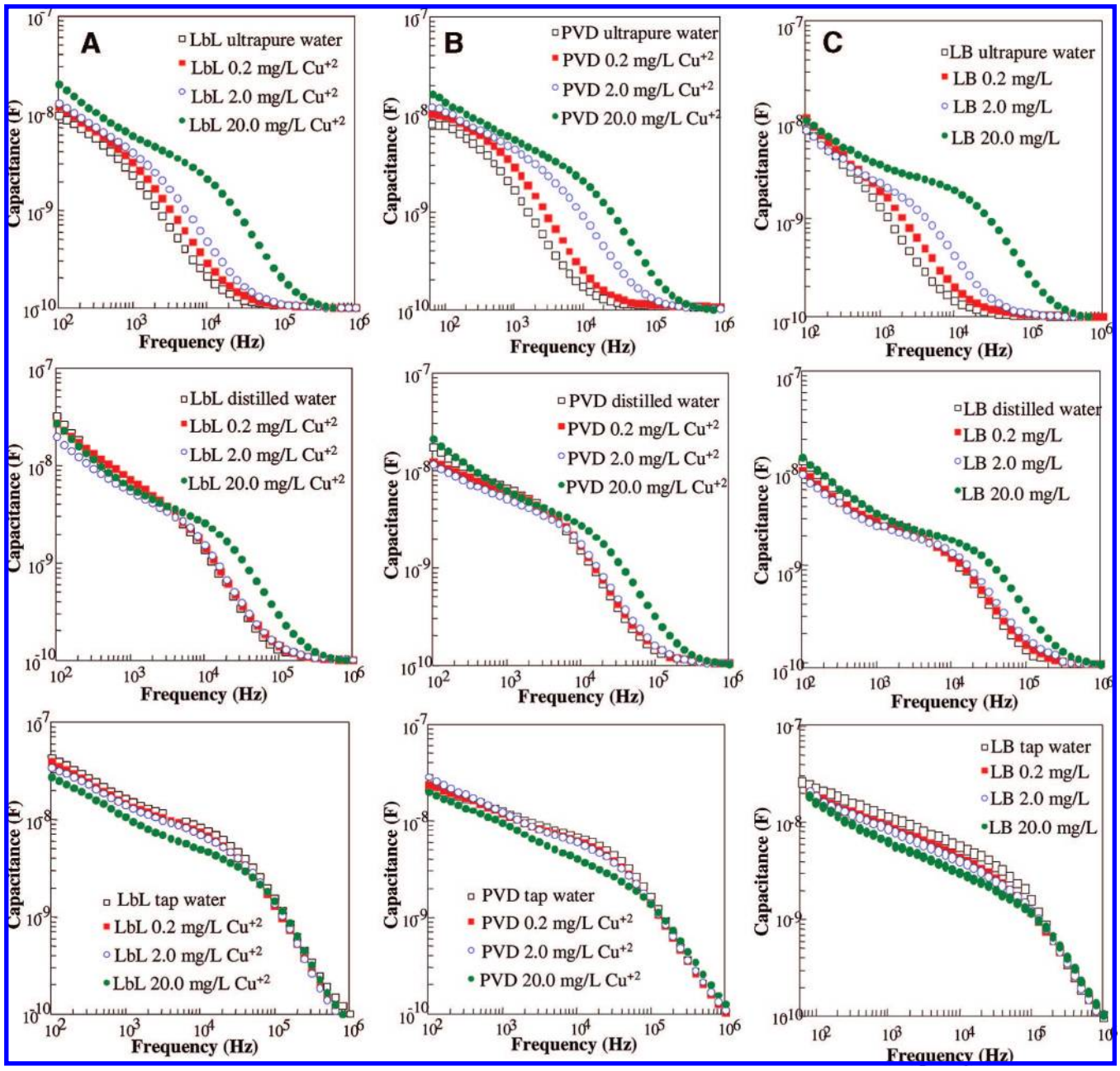

Figure 5. (A) Impedance spectroscopy measurements (capacitance vs frequency) for the five-bilayer PAH/FeTsPc LbL film on Au interdigitated electrodes for different concentrations of Cu^{2+} in ultrapure water, distilled water, and tap water. (B) Impedance spectroscopy measurements (capacitance vs frequency) for the 10 nm FePc PVD film on Au interdigitated electrodes for different concentrations of Cu^{2+} in ultrapure water, distilled water, and tap water. (C) Impedance spectroscopy measurements (capacitance vs frequency) for the five-layer FePc LB film on Au interdigitated electrodes for different concentrations of Cu^{2+} in ultrapure water, distilled water, and tap water.

the sensors, which include impedance spectroscopy that is applied here to assess the possible use of phthalocyanine films in detecting trace amounts of Cu^{2+} ions in aqueous solutions, just as a proof of principle.

Impedance spectroscopy measurements were taken with all sensing units left soaking 20 min in the liquids prior to data acquisition in order to get a stable electrical response. Measurements in ultrapure water were taken before and after each data set in Cu^{2+} solutions to rule out possible contaminations. A careful washing of the sensing units under moderate stirring in ultrapure water was made after exposing the sensor to Cu^{2+} ions. Figure 5 shows capacitance curves of a five-bilayer PAH/FeTsPc LbL film immersed in water and Cu^{2+} solutions at 0.2, 2.0, and 20.0 mg/L prepared with ultrapure, distilled, and tap water. Impedance curves with similar behavior were obtained with 10 nm mass thickness PVD film and five-layer LB film of FePc immersed in the same liquid samples, also illustrated in Figure 5. There was a slight distinction between the lowest concentrations (0.2 and 2.0 mg/L) with ultrapure water. The same applied for tap and distilled water, but with a poorer distinction probably due to the screening effect from a high concentration of other ions in these samples. At 20.0 mg/L the samples were clearly distinguished in all systems.

The data from impedance spectroscopy are rich in terms of information that may allow one to distinguish between very similar samples. A visual inspection of Figure 5 indicates that the capacitance curves shift as the amount of ions in solution varies, which may be caused by changing the Cu^{2+} ion

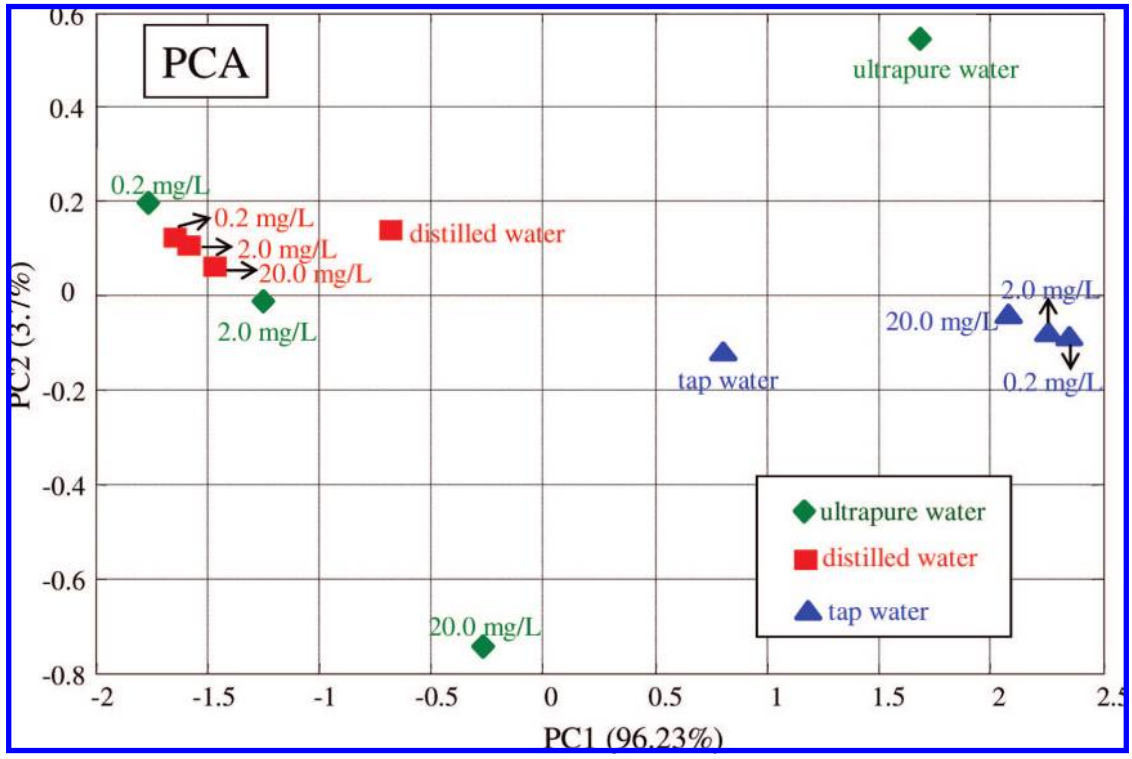

Figure 6. PCA plot for the capacitance values presented in Figure 5A−C at 10 KHz for ultrapure water and at 100 KHz for distilled and tap waters.

TABLE 1: Variation Capacitance Values (ΔC) in pF Collected at 10 kHz for Ultrapure Water and 100 kHz for Distilled and Tap Water

water	LB	LbL	PVD
ultrapure	17.70	21.30	23.10
distilled	4.80	12.00	11.20
tap	3.90	10.80	10.90

concentrations or the type of water used in the experiments. The electrical response is also affected by changes in the films adsorbed onto the interdigitated electrodes and in the electrical double-layer formed at the film/aqueous solution interface. Generally, at a fixed frequency within the 10^3-10^5 Hz range, the capacitance increased with increasing ion concentration in ultrapure and distilled water solutions. For tap water the measured capacitance decreased with increasing ion concentration, apparently due to a shift to higher frequencies in the overall curve when compared to the ultrapure and distilled water. Through computational simulations using the equivalent electric circuit proposed by Taylor and MacDonald,[59] we confirmed this shift in the capacitance curves. For an increase in the ion concentration leads to a reduction in charge transfer and double-layer resistances at the electrode/electrolyte interface, with a concomitant increase in double-layer capacitance, right shifting the curves, as observed experimentally.

It is clear that several features of the curves can be used in distinguishing the samples. Furthermore, the electrical responses from different sensing units may be combined with a statistical method, which has been widely exploited in the so-called electronic tongues,[58] the most sensitive of which have been obtained with impedance spectroscopy and ultrathin films.[60−62] Indeed, we now take advantage of the varied response of the sensing units made with the ultrathin films, as indicated in Figure 5, to verify the distinction ability for the various concentrations of Cu^{2+} ions. We define ΔC as the capacitance difference between measurements taken in water and 20.0 mg/L Cu^{2+} solutions, at 10 kHz for ultrapure water samples and 100 kHz for distilled and tap water samples. These frequencies were chosen so as to maximize distinction of the electric signals (see Table 1). The largest changes appear for ultrapure water, decreasing sequentially for distilled and tap water samples, which actually follows the trend of increasing concentration of impurities. Possibly, the high impurity level in tap water affects Cu^{2+} detection as none of the films used have high specificity to Cu^{2+} ions (possible screening effect allied with low specificity). Principal component analysis (PCA) was used to statistically correlate the samples, whose results are shown in Figure 6. The PCA plot points to a better distinction for solutions made with ultrapure water, probably because it is more susceptible to change with small variations in the samples. Distinction was nevertheless possible for distilled and tap water samples, even at the lowest concentrations of Cu^{2+} measured.

Conclusions

The role of the ultrathin film architecture in the sensing unit performance has been exploited. Ultrathin films of LbL of PAH/FeTsPc and LB and PVD of FePc were fabricated using layer-by-layer, physical vapor deposition, and Langmuir−Blodgett techniques, respectively. The growth of the films was monitored by UV−vis absorption spectroscopy, the morphology investigated through AFM, and the molecular organization of the phthalocyanines in the different films determined by the surface selection rules applied to FTIR spectroscopy in the transmission and reflection modes. The results showed a linear growth of all the films with the number of layers deposited (LbL and LB) or mass thickness evaporated (PVD). The morphology either at micrometer or at nanometer scales revealed that the PVD and LB films present a more homogeneous surface. Besides, in the LbL films the molecules of FeTsPc are randomly organized while in the PVD and LB films FePc has a preferential molecular organization with the macro-ring being tilted in relation to the

substrate surface at different angles. The application of these films in sensing units was carried out through impedance spectroscopy. The measurements were made immerging the sensing units into different types of water (ultrapure, distilled, and tap) containing concentrations of Cu^{2+} below and above drinking water limits. It was shown that a sensor array can be established using sensing units with identical or similar materials simply varying the architectures at nanometer scale of the ultrathin films, revealing the importance of fabrication processes.

Acknowledgment. This work was supported by FAPESP, CNPq (IMMP and CIAM), and CAPES (Brazil). The authors also thank Professor Ricardo F. Aroca from University of Windsor, Canada, by the AFM facilities.

References and Notes

(1) Leznoff, C. C.; Lever, A. B. P. *Phthalocyanines Properties and Applications*; Publishers: Weinheim, Germany, 1989.
(2) Saja, J. A.; Rodriguez-Mendez, M. L. *Adv. Colloid Interface Sci.* **2005**, *116*, 1.
(3) Dini, D.; Hanack, M. *J. Porphyrins Phthalocyanines* **2004**, *8*, 915.
(4) Kempa, A.; Dobrowolski, J. *J. Can. Chem.* **1988**, *66*, 2553.
(5) Nyokong, T.; Isago, H. *J. Porphyrins Phthalocyanines* **2004**, *8*, 1083.
(6) Tang, C. W.; VanSlyke, S. *Appl. Phys. Lett.* **1987**, *51*, 913.
(7) Anderson, T. L.; Komplin, G. C.; Pietro, W. J. *J. Phys. Chem.* **1993**, *97*, 6577.
(8) Zhang, C.; Braun, D.; Heeger, A. J. *J. Appl. Phys.* **1993**, *73*, 5177.
(9) Geiger, F.; Stoldt, M.; Schweizer, H.; Bäuerle, P.; Umbach, E. *Adv. Mater.* **1993**, *5*, 922.
(10) Greenham, N. C.; Moratti, S. C.; Bradley, D. D.; Friend, R. H.; Holmes, A. B. *Nature* **1993**, *365*, 628.
(11) Rella, R.; Serra, A.; Siciliano, P.; Tepore, A.; Valli, L.; Zocco, A. *Supramol. Sci.* **1997**, *4*, 461.
(12) Palacin, S. *Adv. Colloid Interface Sci.* **2000**, *87*, 165.
(13) Battisti, D.; Aroca, R. *J. Am. Chem. Soc.* **1992**, *114*, 1201.
(14) Clavijo, R. E.; Battisti, D.; Aroca, R.; Kovacs, G. J.; Jennings, C. A. *Langmuir* **1992**, *8*, 113.
(15) Zhou, R.; Josse, F.; Gopel, W.; Ozturk, Z. Z.; Bekaroglu, O. *Appl. Organomet. Chem.* **1996**, *10*, 557.
(16) Nitschke, C.; O'Flaherty, S. M.; Kroll, M.; Blau, W. J. *J. Phys. Chem. B* **2004**, *108*, 1287.
(17) Mortimer, R. J.; Dyer, A. L.; Reynolds, J. R. *Displays* **2006**, *27*, 2.
(18) Singh, T. B.; Sariciftci, N. S. *Annu. Rev. Mater. Res.* **2006**, *36*, 199.
(19) Katz, H. E. *Electroanalysis* **2004**, *16*, 1837.
(20) Valli, L. *Adv. Colloid Interface Sci.* **2005**, *116*, 13.
(21) Bouvet, M. *Anal. Bioanal. Chem.* **2006**, *384*, 366.
(22) Petty, M.; Lovett, D. R.; O'Connor, J. M.; Silver, J. *Thin Solid Films* **1989**, *179*, 387.
(23) Gan, L.; Liang, B.; Lu, Z. *Supramol. Sci.* **1998**, *5*, 583.
(24) Burghard, M.; Fischer, C. N.; Schmelzer, M.; Roth, S.; Haisch, P.; Hanack, M. *Synth. Met.* **1994**, *67*, 193.
(25) Gaffo, L.; Constantino, C. J. L.; Moreira, W. C.; Aroca, R. F.; Oliveira, O. N., Jr. *Langmuir* **2002**, *18*, 3561.
(26) Gaffo, L.; Constantino, C. J. L.; Moreira, W. C.; Aroca, R. F.; Oliveira, O. N., Jr. *Spectrochim. Acta A* **2004**, *60*, 321.
(27) Cooper, T. M.; Campbell, A. L.; Crane, R. L. *Langmuir* **1995**, *11*, 2713.
(28) Zhang, X.; Shen, J. *Adv. Mater.* **1999**, *11*, 1139.
(29) Zucolotto, V.; Ferreira, M.; Cordeiro, M. R.; Constantino, C. J. L.; Balogh, D. T.; Zanatta, A. R.; Moreira, W. C.; Oliveira, O. N., Jr. *J. Phys. Chem. B* **2003**, *107*, 3733.
(30) Zucolotto, V.; Ferreira, M.; Cordeiro, M. R.; Constantino, C. J. L.; Moreira, W. C.; Oliveira, O. N., Jr. *Sensors Actuators B* **2006**, *113*, 809.
(31) Aroca, R.; Thedchanamoorthy, A. *Chem. Mater.* **1995**, *7*, 69.
(32) Gaffo, L.; Constantino, C. J. L.; Moreira, W. C.; Aroca, R. F.; Oliveira, O. N., Jr. *J. Raman Spectrosc.* **2002**, *33*, 833.
(33) Treacher, K. E.; Clarkson, G. J.; AliAdib, Z.; McKeown, N. B. *Chem. Commun.* **1996**, *1*, 73.
(34) Ramamurthy, V. *Photochemistry in Organized and Constrained Media*; VCH: New York, 1991.
(35) Debe, M. K. *Prog. Surf. Sci.* **1987**, *24*, 1.
(36) Decius, J. C.; Hexter, R. M. *Molecular Vibrations in Crystals,* McGraw-Hill: New York, 1977.
(37) Greenler, R. G. *J. Chem. Phys.* **1966**, *44*, 310.
(38) Born, M.; Wolf, E. *Principles of Optics*; Pergamon Press: Oxford, 1975.
(39) Bradshaw, A. M.; Schweizer, E. *Spectroscopy of Surface*; John Wiley & Sons: Toronto, Canada, 1988.
(40) Antunes, P. A.; Constantino, C. J. L.; Aroca, R.; Duff, J. *Appl. Spectrosc.* **2001**, *55*, 1341.
(41) See ref 31.
(42) Del Caño, T.; Parra, V.; Rodríguez-Méndez, M. L.; Aroca, R. F.; De Saja, J. A. *Appl. Surf. Sci.* **2005**, *246*, 327.
(43) Yonehara, H.; Etori, H.; Engel, M. K.; Tsushima, M.; Ikeda, N.; Ohno, T.; Pac, C. *Chem. Mater.* **2001**, *13*, 1015.
(44) Sugiyama, K.; Iizuka, S.; Yashir, H.; Fukuda, H.; Shimoyama, Y. *Jpn. J. Appl. Phys.* **2008**, *47*, 492.
(45) Brinkmann, M.; Wittmann, J.-C.; Barthel, M.; Hanack, M.; Chaumont, C. *Chem. Mater.* **2002**, *14*, 904.
(46) Gaffo, L.; Rinaldi, A. W.; Santos, M. J. L.; Girotto, E. M. *J. Porphyrins Phthalocyanines* **2007**, *11*, 618.
(47) Gaffo, L.; Zucolotto, V.; Cordeiro, M. R.; Moreira, W. C.; Oliveira, O. N., Jr.; Cerdeira, F.; Brasil, M. J. S. P. *Thin Solid Films* **2007**, *515*, 7307.
(48) Gorbunova, Y.; Rodriguez-Mendez, M. L.; Kalashnikova, I. P.; Tomilova, L. G.; de Saja, J. A. *Langmuir* **2001**, *17*, 5004.
(49) Cook, M. J. *Pure Appl. Chem.* **1999**, *71*, 2145.
(50) Burghard, M.; Schmelzer, M.; Roth, S.; Haisch, P.; Hanack, M. *Langmuir* **1994**, *10*, 4265.
(51) Rikukawa, M.; Rubner, M. F. *Langmuir* **1994**, *10*, 519.
(52) Souto, J.; De Saja, J. A.; Gobernadomitre, M. I.; Rodríguez, M. L.; Aroca, R. *Sensors Actuators B* **1993**, *16*, 306.
(53) Kumaran, N.; Donley, C. L.; Mendes, S. B.; Armstrong, N. R. *J. Phys. Chem. C* **2008**, *112*, 4971.
(54) Crespilho, F. N.; Zucolotto, V., Jr.; Constantino, C. J. L.; Nart, F. C.; Oliveira, O. N., Jr. *Environ. Sci. Technol.* **2005**, *39*, 5385.
(55) de Souza, N. C.; Zucolotto, V.; Silva, J. R.; Santos, F. R.; Oliveira, O. N., Jr.; Balogh, D. T., Jr.; Giacometti, J. A. *J. Colloid Interface Sci.* **2005**, *285*, 544.
(56) Zucolotto, V.; Ferreira, M.; Cordeiro, M. R.; Constantino, C. J. L.; Moreira, W. C.; Oliveira, O. N., Jr. *Synth. Met.* **2003**, *137*, 945.
(57) Liu, L.; Jin, X.; Yang, S.; Chen, Z.; Lin, X. *Biosens. Bioelectron.* **2007**, *22*, 3210.
(58) Ciosek, P.; Wroblewski, W. *Analyst* **2007**, *132*, 963.
(59) Taylor, D. M.; Macdonald, A. G. *J. Phys., D: Appl. Phys.* **1987**, *20*, 1277.
(60) Ferreira, M.; Riul, A., Jr.; Wohnrath, K.; Fonseca, F. J.; Oliveira, O. N., Jr.; Mattoso, L. H. C. *Anal. Chem.* **2003**, *75*, 953.
(61) Zucolotto, V.; Daghastanli, K. R. P.; Hayasaka, C. O.; Riul, A., Jr.; Ciancaglini, P.; Oliveira, O. N., Jr. *Anal. Chem.* **2007**, *79*, 2163.
(62) da Silva, B. A.; Antunes, P. A.; Pasquini, D.; Curvelo, A. A. S.; Aroca, R. F.; Riul, A., Jr.; Constantino, C. J. L. *J. Nanosci. Nanotechnol.* **2007**, *7*, 510.

JP804159H